MDPI

Article

Wet Ball Milling Applied to Production of Composites and Coatings Based on Ti, W, and Nb Carbides

Marina Eryomina * and **Svetlana Lomayeva**

Udmurt Federal Research Centre of Ural Branch of the Russian Academy of Sciences, T. Baramzinoy St., 34, 426067 Izhevsk, Russia
* Correspondence: mrere@mail.ru

Abstract: The paper demonstrates the potential of wet ball milling of metals for the synthesis of various carbides and carbohydrides. The work reports on multicomponent carbides formed in Ti-(Cu/Fe/Si)-C, W-Fe-C, and Nb-(Cu/Fe/Si/Al)-C systems, as well as metastable or high-temperature intermetallics formed in Ti-Si, Nb-Si, Nb-Al, and Nb-Cu-Fe systems, which are stabilized with interstitial carbon. The formation of phase composition of powders fabricated under mechanochemical synthesis and subsequent thermal treatment has been studied. The as-fabricated powders have been used to produce bulk compacts and to apply wear-resistant coatings on steel (iron).

Keywords: multicomponent carbides; wet ball milling; phase composition; magnetic pulse compaction; high-speed selective laser sintering; hardness; wear resistance

1. Introduction

Transition metal carbides are extensively used in industries owing to their high thermal and chemical stability, appropriate mechanical properties, wear resistance, and catalytic performance [1,2]. Various carbides are used to produce both bulk products and coatings, but the complexity and high cost of the production technologies obstruct their potential use. The development of efficient and low-cost techniques for carbide synthesis is still of high priority.

Mechanical alloying (MA) often uses liquids as a milling medium, among which are water, ethanol, toluene, and other solvents. For MA of metals, the addition of liquid process control agents prevents particle agglomeration and adhesion to milling balls and vials, especially in the case of ductile metals. At the same time, such additives may induce contamination of the milled material with carbon, oxygen, hydrogen, nitrogen, etc., with the respective contaminant elements being involved in the phase formation processes occurring under MA and subsequent thermal treatment. Their influence is often not considered and discussed.

The mechanochemical decomposition of hydrocarbons induced by high-energy ball milling of metals can be successfully used for the synthesis of various carbides, as demonstrated in [3–6]. Under wet ball milling, the products of the medium decomposition are involved in the formation of nanostructured hydrides and carbohydrides. The hydrogen and carbon saturation level of the powder and the hydrogen-to-carbon ratio may be governed by varying milling duration and choosing relevant hydrocarbons. Subsequent thermal treatment provides the removal of stored hydrogen from the material, but the carbides are retained.

This work summarizes our results on carbohydrides and carbides in titanium-, tungsten- and niobium-based systems synthesized via wet ball milling in hydrocarbons and their properties, including hardness and wear resistance of compacts and coatings.

2. Materials and Methods

The study was carried out on powder systems based on titanium, tungsten, and niobium, which are commonly used industrial transition metals. Depending on additional components chosen, MA in the analyzed systems may give varied phase compositions, for example, monocarbide-based compositions in Ti-C and Ti-Cu-C systems or compositions based on multicomponent carbides or mixtures of various carbides in others. Table 1 provides designations of samples, their composition, characteristics of the initial metal powders, and duration of milling in petroleum ether.

Table 1. Initial powder characteristics, elemental composition, and milling duration.

Sample	Initial Powder Composition (wt.%)	Purity and Particle Size	Milling Duration (h) [1]
Ti	Ti–100		1–6
TiCu	Ti–80, Cu–20		1–12
TiFe	Ti–63, Fe–37	Ti—99.02 wt.%, ~40 μm	3–4
TiFeCu	Ti–60, Fe–20, Cu–20	W—99.9 wt.%, 6–20 μm	3–4
TiSi	Ti–83, Si–17	Nb—99.9 wt.%, 6–20 μm	3–4
WFe	W–74, Fe–26	Cu—99.7 wt.%, ~18 μm	6
NbCu	Nb–87, Cu–13	Fe—98.0 wt.%, 3–20 μm	1–7
NbSi	Nb–91, Si–9	Si—98.8 wt.%, ~1000 μm	4
NbAl	Nb–85, Al–15	Al—99.0 wt.%, ~60 μm	1–5
NbAlFe	Nb–72, Al–14, Fe–14		1–5

[1] Significant amounts of Fe contamination for milling longer than 5 h.

The powders were milled using a Fritsch P7 (Fritsch, Idar-Oberstein, Germany) planetary ball mill at a rotation speed of ~700 rpm. A powder mixture of 10 g in total amount was taken for each sample. Milling vials (volume 45 cm^3) and 20 milling balls (8 mm in diameter) were made of hardened steel (1 wt.% C, 1.5 wt.% Cr). Prior to milling, the vials were filled with petroleum ether (analytical grade). The milling for longer than 5 h caused significant abrasion of the milling tools, so the percentage of iron initially added in the sample *WFe* was corrected. In the sample *NbCu*, all iron appears from the abrasion of the milling vials and balls. To analyze temperature-driven changes in the phase composition, the powders milled were annealed at T = 600–1000 °C for 1 h in an argon atmosphere with preliminary pumping down to fore-vacuum pressure. The annealing was carried out in a quartz tube using a laboratory tubular furnace (Pt-Pt 10%Rh-thermocouple, $\Delta T_{max} = \pm 4$ °C). The temperature of annealing was chosen based on the results of differential thermal analysis (STA8000, 20 °C/min).

After milling, the powders were (1) compacted and (2) applied as coatings to plates made of steel *A* (0.12 wt.% C, 18.0 wt.% Cr, 3.0 wt.% Ni), steel *B* (0.87 wt.% C, 0.51 wt.% Mn, 0.34 wt.% Si), and Armco iron (Armco Inc., Middletown, OH, USA).

The compacts were prepared via magnetic pulse compaction [7] at 500 °C in a vacuum (residual pressure 5–10 Pa) with preliminary degassing for 4 h at the same temperature. The amplitude of pressure pulses was ~1.5 GPa, with a duration of 300 μs. The resulting compacts were disks 10 mm in diameter and 3–4 mm thick. The coatings were applied via high-speed selective laser sintering (SLS) [8] using a Nd:YAG laser (λ = 1.065 μm, power 50 W, frequency 50–100 kHz, scanning speed 20–100 mm/s) in an argon atmosphere, with the beam focus of 30 μm in diameter.

X-ray diffraction (XRD) analysis of the samples was carried out from 10° to 140° with a MiniFlex600 X-ray diffractometer (Rigaku, Tokyo, Japan) in CoKα radiation. Qualitative and quantitative phase analyses were performed using the PDF-2 database and the PHAN% software [9] based on the full-profile Rietveld refinement of the measured XRD patterns, respectively. Scanning electron microscope (SEM) images were taken using a Thermo Fisher Scientific (FEI, Hillsboro, OR, USA) Quattro S and VEGA 3 LMN (TESCAN, Brno, Czech Republic) equipped with an energy-dispersive analysis device.

The density of compacts was evaluated by hydrostatic weighing using a CE 224 C weighing device (Sartogosm, Saint Petersburg, Russia) equipped with a YDK 03 attachment (Sartorius, Göttingen, Germany). The Vickers hardness was measured on a PMT-3 device with ten measurements at a load of 0.98 N. The lubrication-free friction parameters were obtained using the vibration module of an Optimol SRV-III Test System friction machine (Optimol, Brussels, Belgium), with balls made of hardened steel (1 wt.% C, 1.5 wt.% Cr, diameter 9.4 mm, hardness 55–57 HRC) or WC-6Co alloy (diameter 9.5 mm, hardness 89 HRA) as counterbodies. The load on the counterbody was 10 N, with the range of movement of the counterbody being 3 mm. The oscillation frequency was 10 Hz (0.06 m/s), and the duration was 10 min. The measurements were carried out at room temperature and 30% humidity.

3. Results and Discussion

3.1. Titanium-Based Systems

While the properties of titanium carbide and hydride are well known, titanium carbohydrides are still not studied enough. Titanium carbohydrides having *fcc* and *hcp* structures are prepared by sintering titanium and carbon powders in the presence of hydrogen at 1000–1100 °C [10,11] or via MA in hydrocarbons [12,13]. Carbohydrides are attractive because of their potential application in the aviation and medical industries. Nevertheless, there are published data for only titanium carbohydrides of the *fcc* structure [10], while the properties of titanium carbohydrides of the *hcp* structure have not been studied so far, except for their thermal stability.

MA of titanium powder in petroleum ether induces structural phase transformations in titanium starting from its transition to a nanostructured state and progressing to the formation of a solid solution of carbon and hydrogen in the α-Ti (ICSD#1-1197) and then the formation of titanium hydride TiH_2 (ICSD#3-859) and metastable titanium carbohydride Ti(C,H) (ICSD#65-8746) with the *fcc* lattice similar to that of titanium carbide (Sample *Ti*, Figure 1a). XRD analysis reveals the formation of Ti(C,H) starting from 2 h of milling. After 4 h of milling, all titanium enters the composition of the Ti(C,H) + TiH_2 mixture. The broadening of the XRD reflections observed for the solid solution, titanium hydride, and titanium carbohydride indicates a nanostructured state and substantial structural disordering. The grain size (coherent scattering region diameter) is 2–4 nm. The particle size of the powder after 4 h of milling ranges from 2–5 μm to 50 μm in agglomerates (Figure 1b). The particle shape is stone-like in this case and in all the systems described below.

Annealing of the resulting powder at 600 °C causes the decomposition of metastable Ti(C,H) carbohydride of *fcc* lattice and the formation of more stable titanium carbohydrides of *hcp* lattice with a composition close to $Ti_2CH_{0.6}$ [14] and of *fcc* lattice with a higher carbon content [15] (Figure 2a). Annealing at 900 °C induces its complete decomposition with the formation of non-stoichiometric titanium carbide $TiC_{0.48}$ (ICSD#6-614) and a mixture of α-Ti and β-Ti (ICSD#44-1288). Evidently, β-Ti is stabilized by iron impurities (Figure 1c). After annealing, the lattice parameter of the Ti(C,H) decreases from ~4.299 Å to 4.284 Å because of hydrogen release.

The milled powders were compacted to prepare compacts based on titanium carbohydride $Ti_2CH_{0.6}$ (Figure 2a) [16]. To retain the titanium carbohydride phase in the composition, the powders are to be compacted at temperatures not higher than 700–800 °C, which makes magnetic pulse compaction the most appropriate technique for fabricating high-density samples [8]. The hardness of the *Ti* compacts based on the *hcp* titanium carbohydride is about 4 GPa, and the density is 4.0 g·cm^{-3} (Table 2). Such a combination of hardness and density makes the prepared compact even better than a commercial Ti-6Al-4V alloy showing a density of 4.42–4.47 g·cm^{-3} and a Vickers hardness of 3.3–3.6 GPa [17].
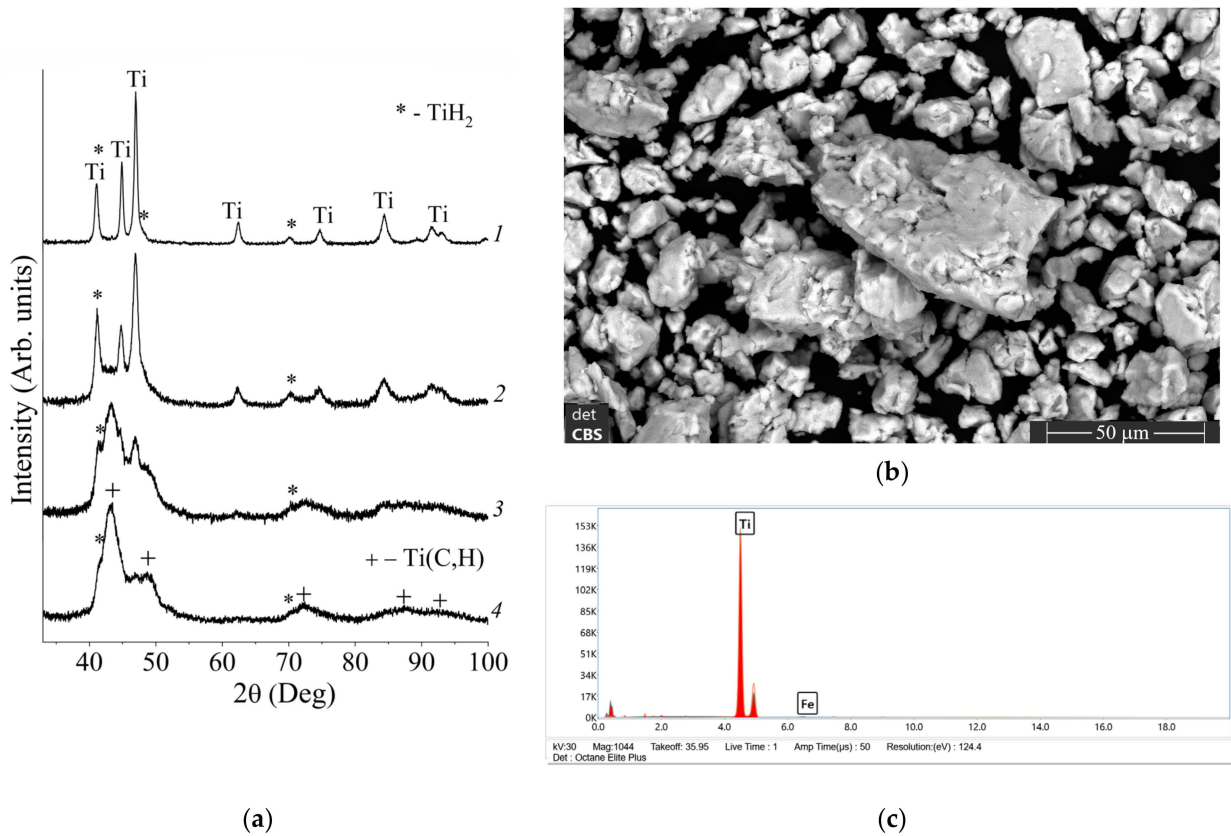
Figure 1. (**a**) XRD patterns of powders (sample *Ti*) milled for (1) 1 h, (2) 2 h, (3) 3.5 h, (4) 4 h; (**b**) SEM image and (**c**) EDX spectrum of the powder (sample *Ti*) milled for 4 h.
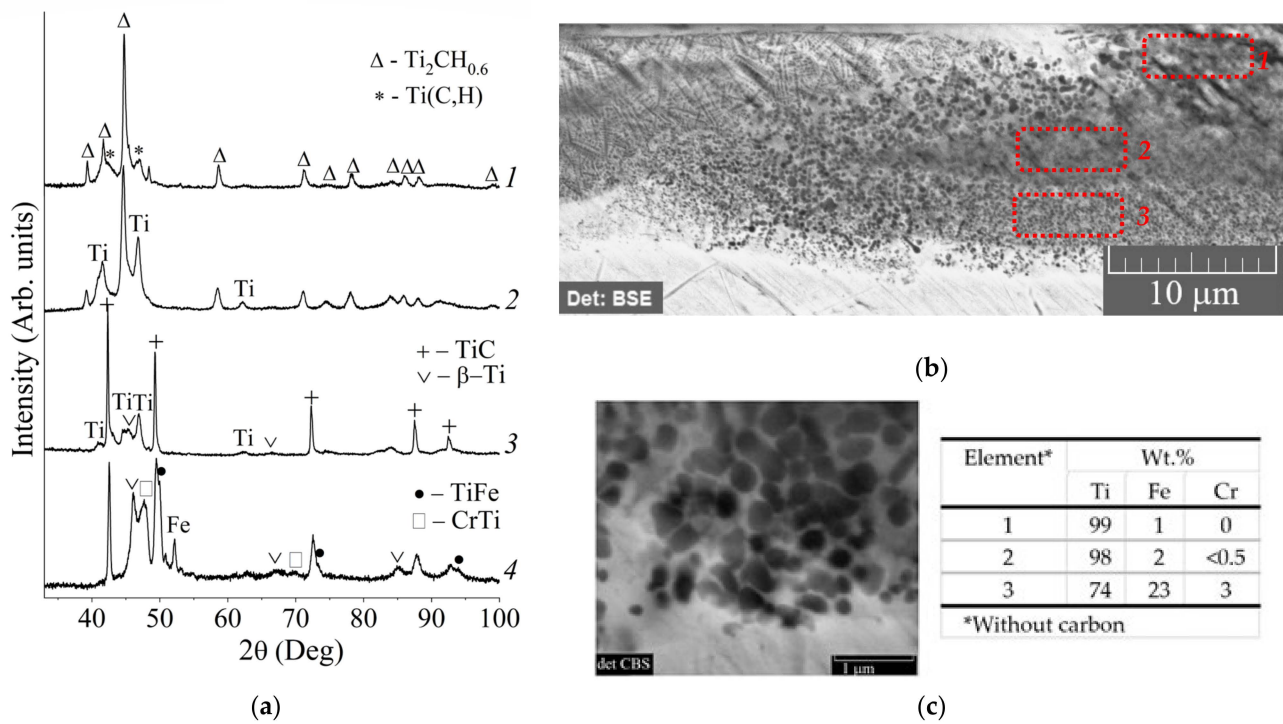
Figure 2. (**a**) XRD patterns of sample *Ti*: (*1*, *3*) MA powder annealed at (*1*) 600 °C and (*3*) 900 °C; (*2*) compact; (*4*) coating; (**b**,**c**) SEM images and elemental composition of coating *Ti*. MA duration is 4 h.

**Table 2.** Properties of compacts and coatings.

Sample Designation		Ti		TiCu		WFe		NbCu	
		Compact	Coating	Compact	Coating	Compact	Coating	Compact	Coating
Density (±0.01 g·cm^{-3})		4.00	-	4.60	-	11.93 (as prepared) 10.70 (annealed)	-	7.1	-
HV (GPa)		4.1 ± 0.5	10.0 ± 1.7	5.1 ± 0.8	8.3 ± 0.3	6.2 (as prepared) 7.9 (annealed)	16.0 ± 2.0	3.8 ± 0.4	10.8 ± 1.9
Friction coefficient (±0.01) with steel ball	Initial	0.2	0.15	0.6	0.15	-	0.20	-	0.25
	Max	1.5–2	0.20	1.24	0.40	-	0.28	-	0.90
Wear of sample/steel ball (±1 μm)		125/0	0/17	6/38	0/47	-	0/1	-	0/7
Friction coefficient (±0.01) with WC-6Co ball	Initial	-	0.15	-	0.17	0.05 (annealed)	0.06	-	0.29
	Max	-	0.16	-	0.30	0.45 (annealed)	0.22	-	0.70
Wear of sample/WC-6Co ball (±1 μm)		-	0/3	-	3/16	0/1 (annealed)	0/0	-	0/4

When *Ti* coating is applied to steel plates *A*, hydrides and carbohydrides decompose, and the released titanium interacts with the melted steel substrate to form carbide, intermetallic compounds, and solid solutions [18,19]. The resulting gradient coating is 10 μm thick and turns out to be well attached to the substrate. Carbides are formed as rounded inclusions of 50–100 nm in size and dendrites of up to 5 μm in length, and the inclusions are surrounded by a shell of intermetallic compounds of up to 50 nm thick (Figure 2b). Nanosized carbide inclusions, covered with an intermetallic shell that gives strong bonding with the substrate, provide high hardness (~10 GPa) and high wear resistance under lubrication-free dry friction at a load of 10 N. The friction coefficients in tribopairs are not higher than 0.2. Thus, the wear resistance of the coating under dry friction is comparable with that of an industrial sintered alloy based on tungsten carbide. The short duration required for both the mechanical treatment and the subsequent application of the coatings, together with their low cost, makes this method one of the most effective as compared to tungsten carbide-based alloys.

The composites based on carbohydride and/or titanium carbide were prepared with copper as a binder [16]. Copper is chosen as a non-toxic metal, in contrast to cobalt, and possesses bactericidal properties. In addition, copper has high thermal and electrical conductivity and is easy to process. MA of titanium and copper in petroleum ether (Figure 3a,b, sample *TiCu*) for 3 h gives a mixture of metastable titanium carbohydride and intermetallic phases (Figure 3b). Further MA increases the concentration of carbon in the carbohydride and the proportion of abrasive iron. The Ti(C,H) lattice parameter increases from ~4.298 Å to 4.315 Å with milling time. The particle size is 5 to 50 μm after 3 h milling and 1 to 10 μm after 6 h milling (Figure 4a–c). Annealing at 600 °C of the 4 h milled powder gives a mixture of the *hcp* Ti$_2$CH$_{0.6}$ and CuTi$_2$ (ICSD#18-458) intermetallic, while annealing at 900 °C gives a mixture of non-stoichiometric TiC$_{0.5}$ and intermetallic CuTi$_2$ (type *A6*) and TiFe (ICSD#65-7743) (Figure 3b). XRD analysis revealed iron in the sample only after annealing at 900 °C, since a noticeable increase in the grain size of iron or iron-containing phases may be provided only at 700 °C or above (0.4 of T$_m$).

The *TiCu* compacts based on the titanium carbohydride Ti$_2$CH$_{0.6}$ and CuTi$_2$ intermetallic have a layered structure [20,21], with a layer thickness of 50–100 nm (Figure 5a). The intermetallic present in the phase composition provides higher density (4.6 g·cm^{-3}), hardness (5.1 GPa), and wear resistance of these compacts as compared to the *Ti* compacts (Table 2).
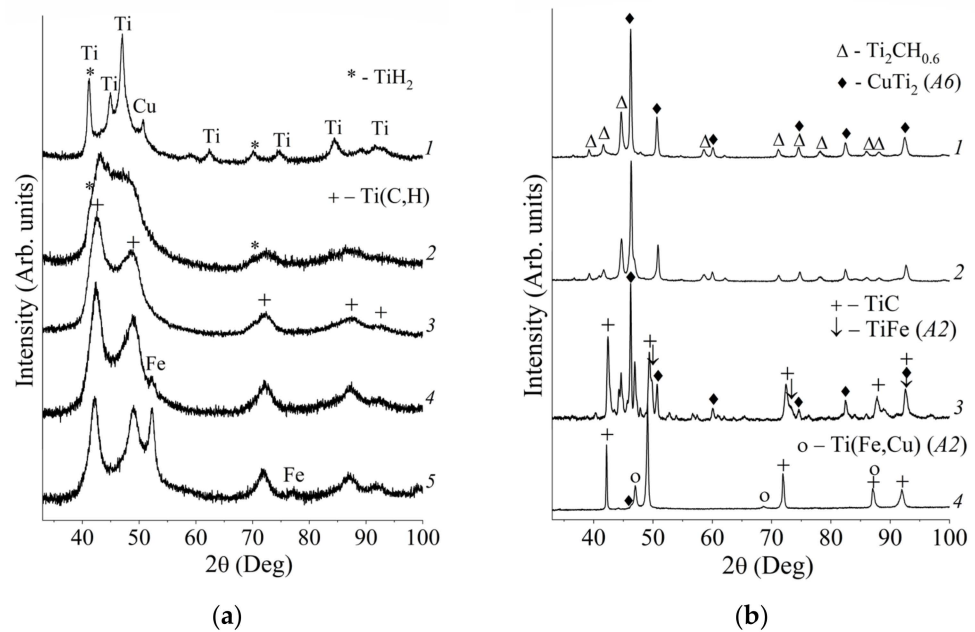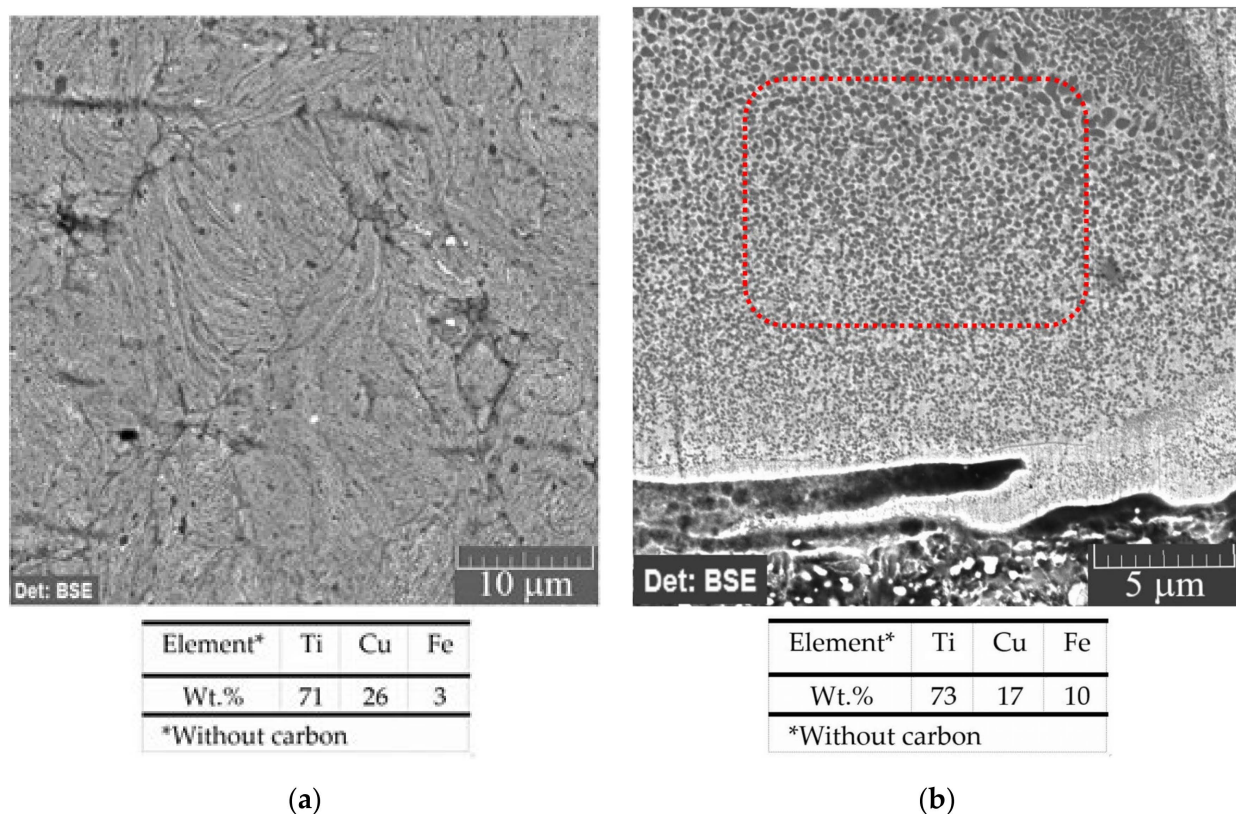
Figure 3. XRD patterns of powders: (**a**) sample *TiCu* milled for (*1*) 1 h, (*2*) 3 h, (*3*) 4 h, (*4*) 6 h, (*5*) 12 h; (**b**) sample *TiCu*: (*1*, *3*) 4 h milling followed by annealing at (*1*) 600 °C and (*3*) 900 °C; (*2*) compact made from 4 h milled powder; (*4*) coating made from 6 h milled powder.
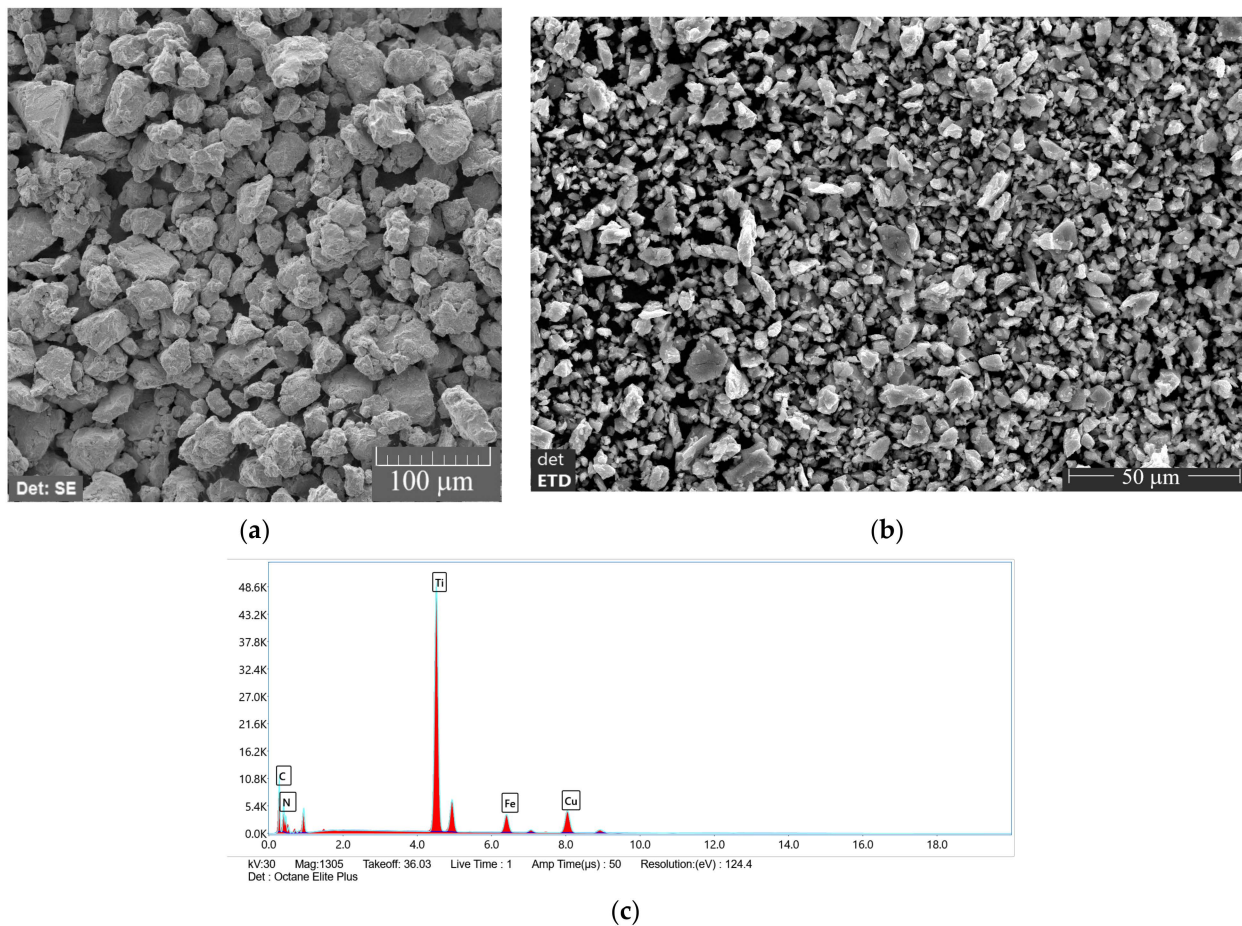
Figure 4. (**a**) SEM image of the MA powder (sample *TiCu*). MA duration is 3 h. (**b**) SEM image and (**c**) EDX spectrum of the MA powder (sample *TiCu*). MA duration is 6 h.

Figure 5. (**a**) SEM image and elemental composition of compact *TiCu*. MA duration is 3 h. (**b**) SEM image and elemental composition of coating *TiCu*. MA duration is 6 h.

The *TiCu* coatings applied to steel plate *B* are composed of $TiC_{0.55}$ and an intermetallic with the *bcc* lattice of type *A2*, similar to the TiFe intermetallic with copper dissolved in it, Ti(Fe,Cu) (Figure 3b). The coating thickness is 40 µm, the hardness is 8.3 GPa, and the friction coefficient is 0.4 and 0.3 for steel and WC-6Co balls, respectively (Table 2). The coating is not worn under dry friction with a steel ball, whereas under dry friction with a WC-6Co ball, the carbide ball is worn to a greater degree than the coating. High hardness and wear resistance of the coatings is provided by a disperse microstructure with carbide inclusions ranging from 100 nm to 1 µm in size and strong adhesion between the coating and the substrate (Figure 5b).

MA of Ti-based powder systems with the use of steel tools (vials and balls) is accompanied by unavoidable abrasion of balls and vials resulting in Fe contamination of the powders milled. The inevitable Fe contamination may be efficiently used to improve the properties of the composites, as Ti-Fe intermetallics and multicomponent Fe-containing carbides are known to have a very high hardness. As mentioned above, the *TiCu* compact contains an intermetallic similar to TiFe. To reveal phase formation processes occurring in this system, titanium–iron (sample *TiFe*) and titanium–iron–copper (sample *TiFeCu*) powders were also milled.

Annealing of the milled powders at 900–1000 °C induces the formation of the Ti_4Fe_2X phase having the cubic lattice of $Fd\bar{3}m$ type with parameters of 11.362 and 11.312 Å for samples *TiFe* and *TiFeCu*, respectively (Figure 6a). The existence of phases with the $Fd\bar{3}m$ type structure, similar to η-carbides, in ternary Ti-Fe-O and Ti-Cu-O systems has been previously shown experimentally [22]. As suggested in [23], the Ti_4Fe_2 phase may be stabilized by nitrogen impurities (ICSD#84-1687). In our case, the phase stabilization is provided by carbon.
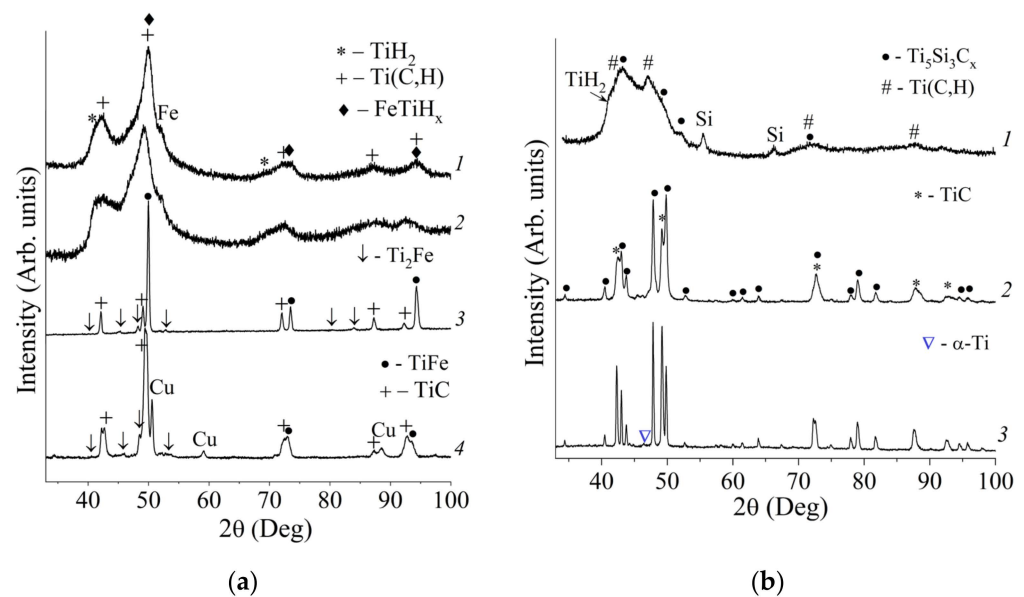
Figure 6. (**a**) XRD patterns of (*1, 2*) MA powders and (*3, 4*) powders annealed at 900 °C for samples (*1, 3*) *TiFe* and (*2, 4*) *TiFeCu*; (**b**) XRD patterns of (*1*) MA powders and (*2, 3*) annealed powders for sample *TiSi*: (*2*) 900 °C, (*3*) 1000 °C. MA duration is 4 h.

Stabilization of metastable phases by carbon has been demonstrated in our earlier work [24] devoted to wet ball milling of titanium and silicon powders. The formation of the $Ti_5Si_3C_x$ phase, which is a high-temperature carbon-stabilized variety of Ti_5Si_3 (ICSD#29-1362) intermetallic having the *hcp* lattice of $D8_8$ type [22], begins after 4 h of milling (sample *TiSi*, Figure 6b). Annealing of powders at 900–1200 °C gives a two-phase mixture, $Ti_5Si_3C_x$ + TiC. The addition of copper and iron to the Ti-Si alloy leads to the appearance of phases with the structure of η-carbides.

In summary, MA in liquid hydrocarbons is a promising method for the synthesis of composites based on carbon interstitials difficult to prepare as single phases via conventional methods.

3.2. Tungsten-Based Systems

MA of tungsten and iron in petroleum ether was used to synthesize η-carbides in the W-Fe-C system (sample *WFe*, Figure 7a) [25]. Since milling tools (vials and balls) are made of hardened steel, nanostructured Fe contamination is involved in the formation of carbides. In tungsten-based systems, hydrides are not stable at normal pressure. Tungsten carbohydride is not formed, in contrast to titanium- and niobium-based systems, where carbohydride results from the saturation of hydride with carbon. So, MA gives a metastable solid solution of iron and carbon in tungsten, which then decomposes into one/two η-carbides, $(W,Fe)_6C$ (ICSD#3-980) and/or $(W,Fe)_{12}C$ (ICSD#23-1127) (sample *WFe*, Figure 7a,b), under subsequent annealing at above 770 °C. The particular type of phase depends on the carbon concentration accumulated from the milling medium and on the heat treatment conditions. Annealing at 900 °C gives $(W,Fe)_{12}C$, while the compact annealed at the same temperature is of two phases, $(W,Fe)_6C$ + $(W,Fe)_{12}C$.

The powder particle size is 0.5–8 μm and up to 25 μm in agglomerates (Figure 8a,b). The microstructure of the *WFe* compacts is quite homogeneous, with tungsten inclusions as large as 200 nm being visible within the nanosized carbide matrix (Figure 8c).
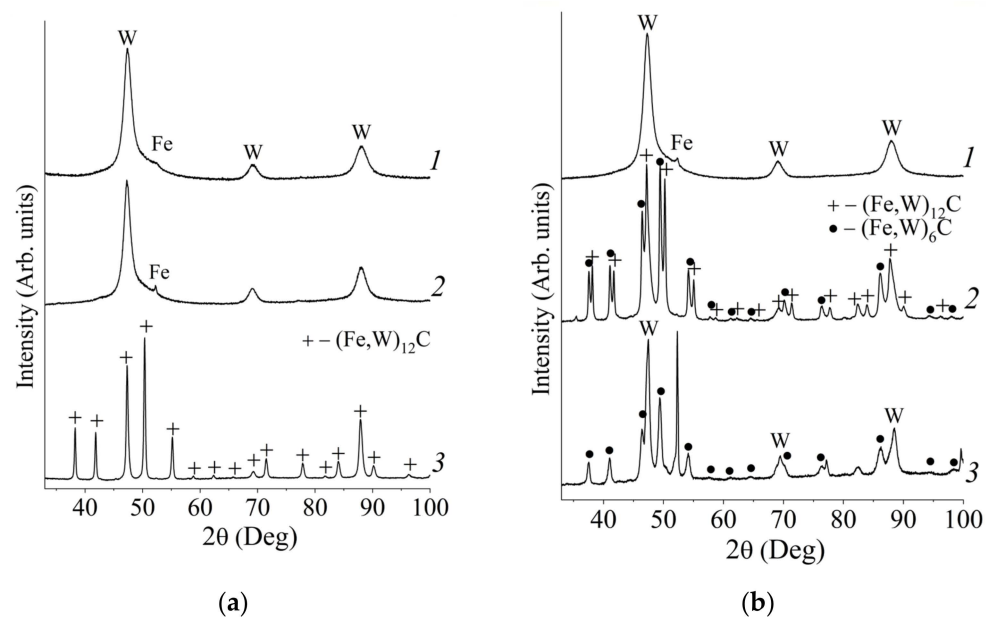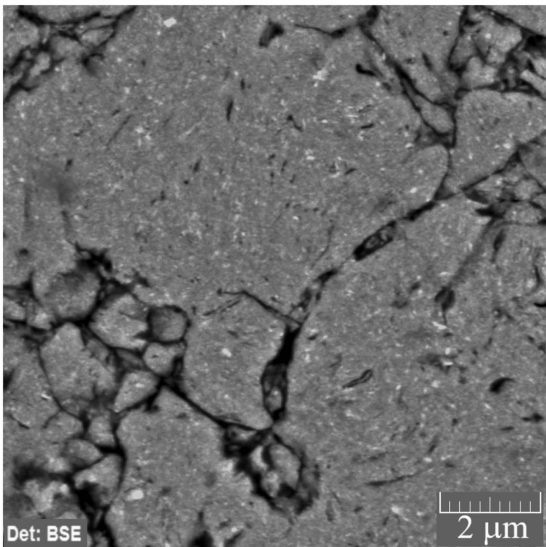
Figure 7. (**a**) XRD patterns of sample *WFe*: (*1*) MA powder, (*2*) heated to 765 °C, (*3*) annealed at 900 °C. MA duration is 6 h. (**b**) XRD patterns of sample *WFe*: (*1*) compact; (*2*) compact annealed at 900 °C; (*3*) coating. MA duration is 6 h.
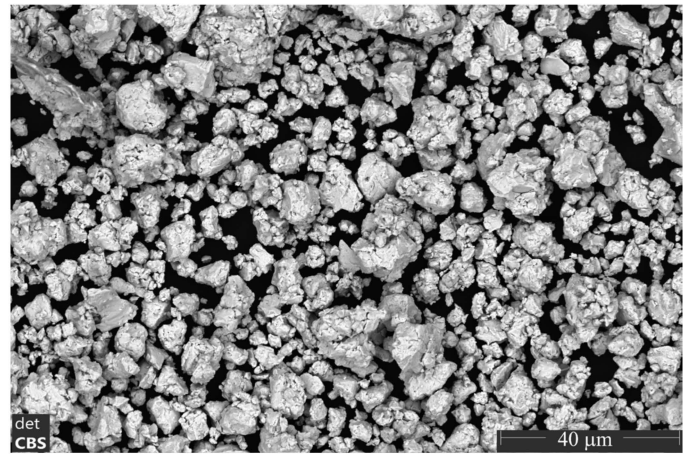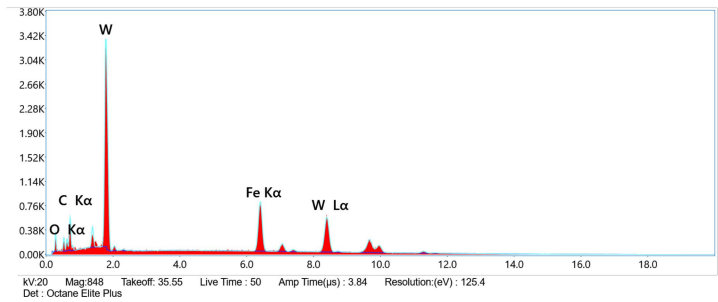

| Element*	W	Fe
Wt.%	67	33
*Without carbon		

Figure 8. (**a**) SEM image and (**b**) EDX spectrum of the MA powder (sample *WFe*). MA duration is 6 h. (**c**) SEM image and elemental composition of the compact (sample *WFe*). MA duration is 6 h.

The *WFe* compact before and after annealing has a density of 11.9 and 10.7 g·cm^{-3}, respectively, with the respective values of hardness being 6.2 and 7.9 GPa (Table 2). The compact is not worn out under a dry sliding wear test with a WC-6Co ball. The friction coefficient is equal to 0.45.

The *WFe* coatings applied to Armco iron plates are composed of two main phases, $(W,Fe)_6C$ and tungsten [26,27]. The coating contains carbide inclusions ranging from 40 to 500 nm (Figure 9a–c) and having a variable composition, with a tungsten-enriched central part and iron-enriched periphery. This structure provides better cohesion between the carbide grain and iron matrix, as well as high hardness and wear resistance. The coating thickness is about 70 μm, and the hardness is ~16 GPa (Table 2). The obtained hardness value makes this coating similar to WC and WC + W_2C coatings (16–24 GPa) [28,29]. Tribological tests showed no signs of wear in the tribopair "*WFe* coating/WC-6Co alloy ball", whereas titanium coatings revealed noticeable wear of the ball. The production of bimetallic carbides is lower-cost, and they may successfully replace tungsten monocarbides and subcarbides in some cases.


(**a**)

(**b**)

(**c**)
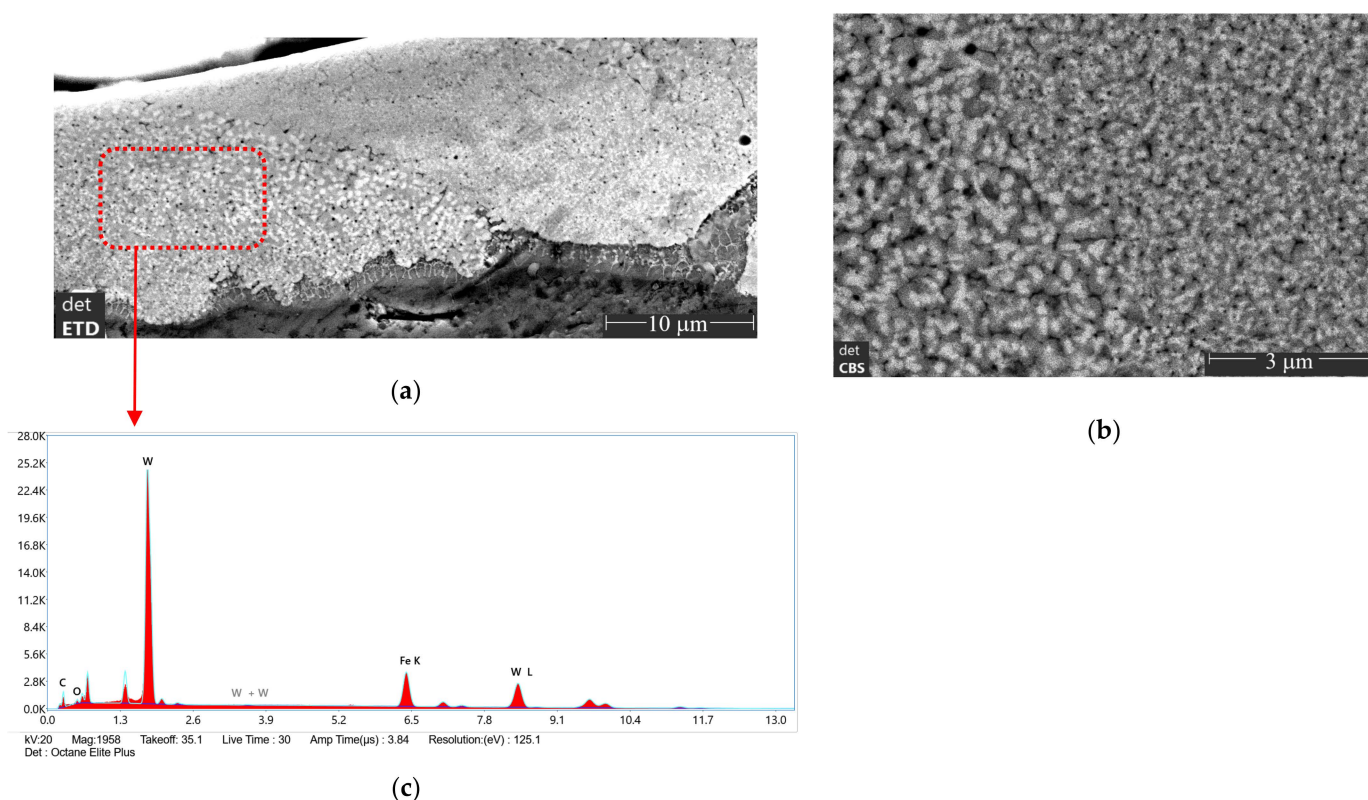
Figure 9. (**a**,**b**) SEM image and (**c**) EDX spectrum of the coating (sample *WFe*). MA duration is 6 h.

3.3. Niobium-Based Systems

MA in hydrocarbons is also efficient in the synthesis of η-carbides and carbon-stabilized intermetallics in niobium-based systems. Co-milling of niobium and copper powders in petroleum ether gives a metastable solid solution of carbon and hydrogen in niobium at the initial stage, which is followed by the formation of niobium hydride $NbH_{0.9}$ (ICSD#7-263) by 3 h of milling [20]. By 6–7 h of milling, metastable niobium carbohydride (ICSD#89-7435) is formed, which has the *fcc* structure close to NbC (sample *NbCu*, Figure 10a). The lattice parameter of Nb(C,H) is equal to 4.411(1) Å. The particle size of the 7 h milled powder is ~5 μm, with agglomerates of 20–50 μm in size (Figure 10b,c). Abrasion of steel milling tools results in the appearance of reflexes from iron in the XRD patterns. The absence of any reflexes from copper in the XRD patterns points to the probable replacement of niobium atoms in the metastable carbohydride with copper. Copper may also be retained in the

X-ray amorphous phase. In addition, an amorphous halo is also conceivable in the observed XRD patterns (Figure 10a, curves *1, 2,* and *4*). Further research is required to clarify this.
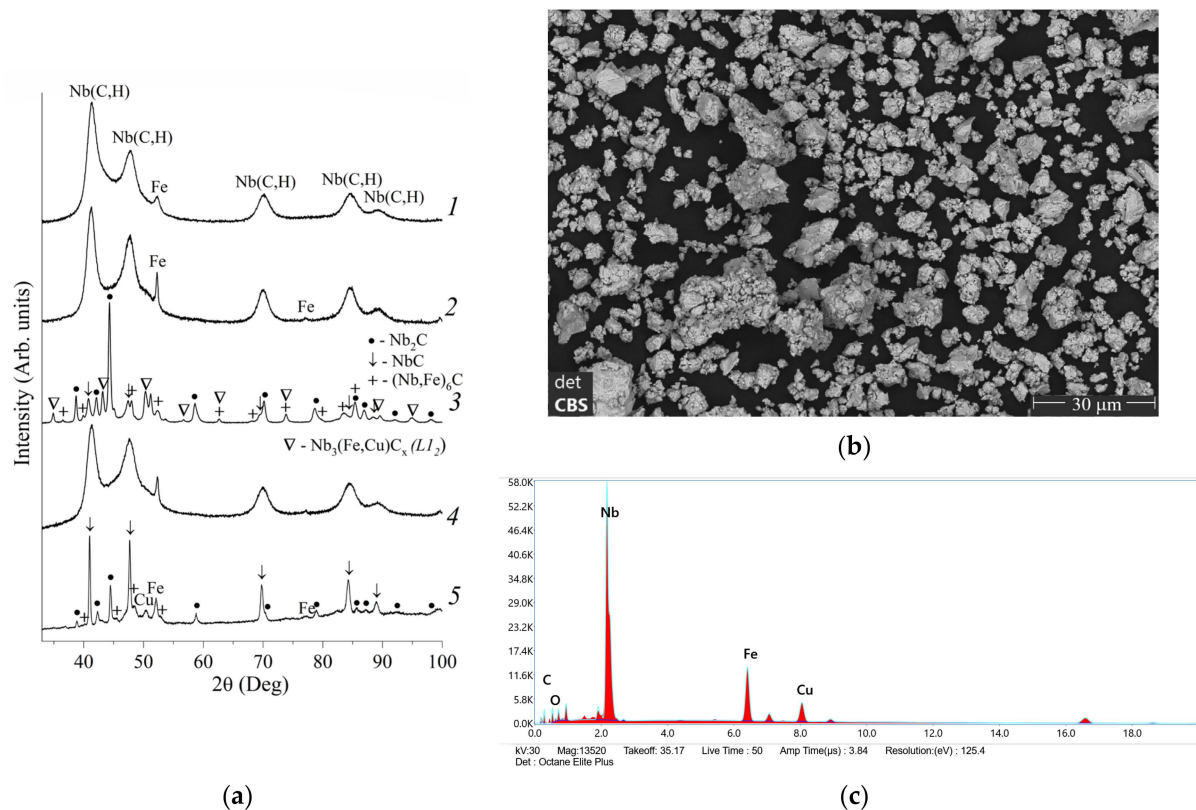

Figure 10. (**a**) XRD patterns of sample *NbCu*: (*1*) MA powder; (*2, 3*) MA powder annealed at (*2*) 600 °C and (*3*) 900 °C; (**4**) compact; (**5**) coating. (**b**) SEM image and (**c**) EDX spectrum of the MA powder (sample *NbCu*). MA duration is 7 h.

Since thermal dehydrogenation of the niobium carbohydride powder occurs at temperatures below 400 °C, the powder annealed at 600 °C does not contain hydrogen. The lattice parameter of NbC is equal to 4.404(1) Å, which indicates the formation of a metastable copper-containing carbide phase.

The metastable niobium phase decomposes at 900 °C into Nb_2C (ICSD#15-127), NbC (ICSD#5-658) with the lattice parameter of 4.445(1) Å, $(Fe,Nb)_6C$ (ICSD#17-128) carbides [30,31], and a phase with the $L1_2$ structure (Cu_3Au type). A phase with the $L1_2$ structure is apparently $Nb_3(Fe,Cu)C_x$ with the lattice parameter of 4.209(1) Å. The Nb_3Fe phase of the same type has a lattice parameter of 4.04 Å [32], while the lattice parameters of Nb_3Cu of the $L1_2$ structure which exists at high pressures are 4.05 Å or 4.08 Å [33,34]. It is known that various unstable structures of Cu_3Au type are stabilized in the presence of interstitial B, C, and N atoms [35]. The absence of other copper-containing phases in the measured XRD pattern and the presence of a larger lattice parameter support the partial replacement of iron with copper in the resulting phase. The formation of the $Nb_3(Fe,Cu)C_x$ phase has not been observed and reported elsewhere before; it is synthesized for the first time. The formation of this phase can be caused by the transformation and ordering process of the metastable *fcc* phase into $L1_2$ or the decomposition of the XRD amorphous phase.

The *NbCu* compact based on a metastable niobium carbide-like phase (Figures 10a and 11a) has a density of 7.1 g·cm^{-3}. Its hardness is 3.8 GPa (Table 2), which is close to that observed for *Ti* compacts.
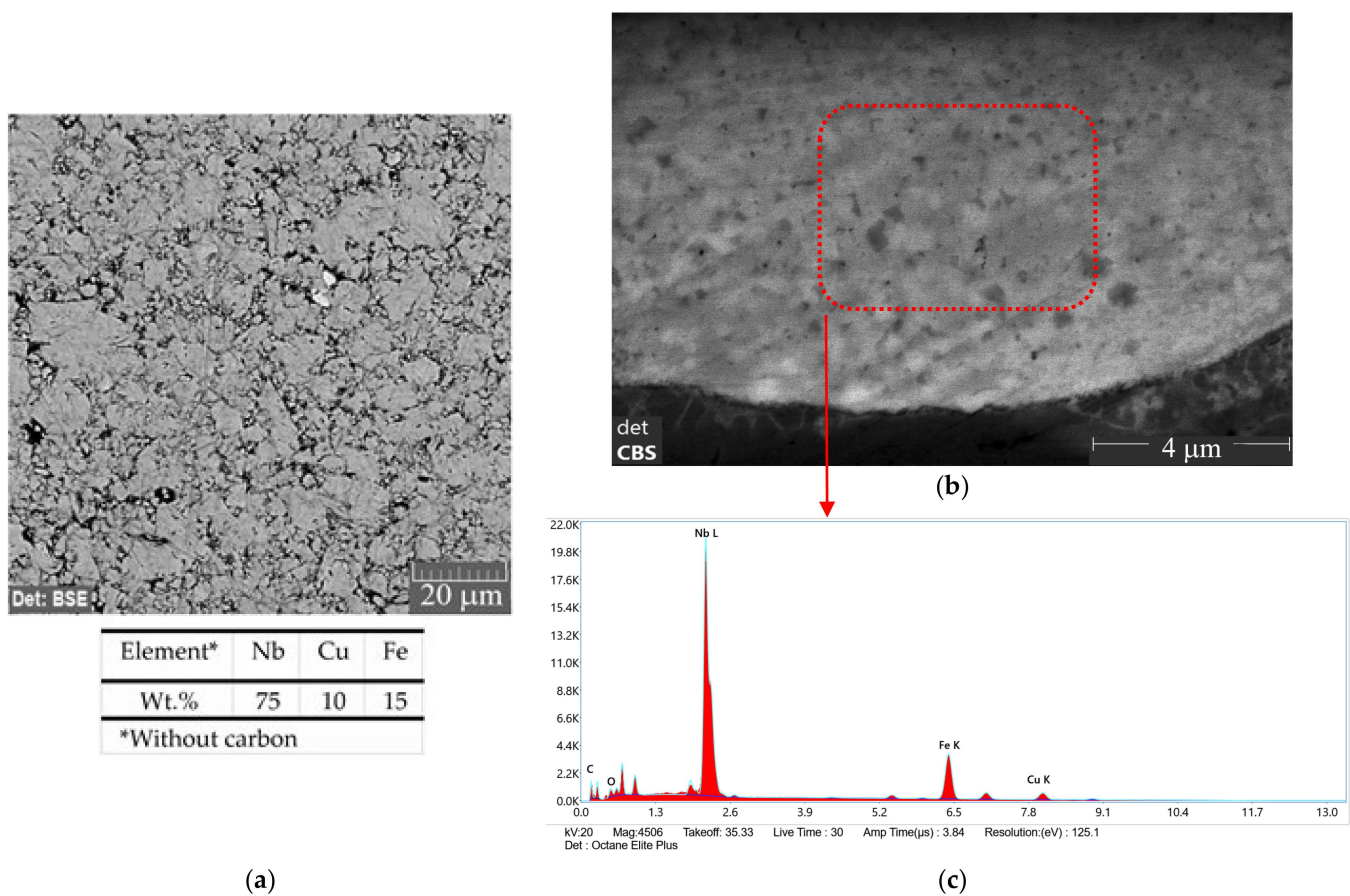
Figure 11. (**a**) SEM image and elemental composition of the compact *NbCu*. MA duration is 7 h. (**b**) SEM image and (**c**) EDX spectrum of the coating *NbCu*. MA duration is 7 h.

The *NbCu* coating applied to the Armco iron plate is mainly composed of niobium monocarbide and subcarbide, with η-carbide $(Nb,Fe)_6C$ being formed and copper being retained (Figure 10a). The coating thickness is 10 μm, and its hardness is up to 10.8 GPa, which is close to that of the *Ti* coatings. The microstructure of the coating is homogeneous, with carbide inclusions ranging from 50 to 500 nm (Figure 11b,c). The coating is wear-resistant and is not worn out under dry sliding with a WC-6Co alloy ball [30].

MA of Nb-Si in petroleum ether gives a metastable supersaturated solid solution of alloying elements in niobium and niobium hydride phase $NbH_{0.9}$ by 4 h of milling, which decomposes under annealing at 900 °C into niobium subcarbide Nb_2C, carbon-stabilized niobium silicide $Nb_5Si_3C_x$ ($D8_8$) (ICSD#65-3599), and Nb_3SiC_x with the $L1_2$ structure (sample *NbSi*, Figure 12). The Nb_3Si (ICSD#15-630) silicide with the $L1_2$ structure is considered to be unstable [36], but it is stabilized in the presence of interstitial carbon [22,37]. Annealing at 1300 °C induces its decomposition into η-carbide $(Nb,Fe)_6C$ and the Nb_4SiFe (ICSD#18-647) intermetallic.

Wet ball milling in liquid hydrocarbons makes it possible to stabilize metastable phases with carbon in Nb-Al-C and Nb-Fe-Al-C systems. In the niobium–aluminum system, the initial stage of milling proceeds with the formation of niobium hydride and a supersaturated solid solution of alloying elements in niobium. Annealing at 900 °C gives $Nb_5Al_3C_x$ with the $D8_8$ type structure (sample *NbAl*, Figure 13a). This phase has been previously obtained only as a thin epitaxial layer [38], but its preparation as a bulk has been considered not possible. $Nb_5Al_3C_x$ is formed from a supersaturated solid solution of other elements in niobium, probably through the transformation of a *bcc* solid solution ($Im\bar{3}m$) to a metastable phase with *B2* structure ($Pm\bar{3}m$, $L1_2$) [39] and then its subsequent decomposition accompanied by the formation of hexagonal phase $Nb_5Al_3C_x$, similar to

that described for Ti-45Al-8.5Nb-(W, B, Y) alloy [40]. The hexagonal phase is stabilized by intercalated carbon.
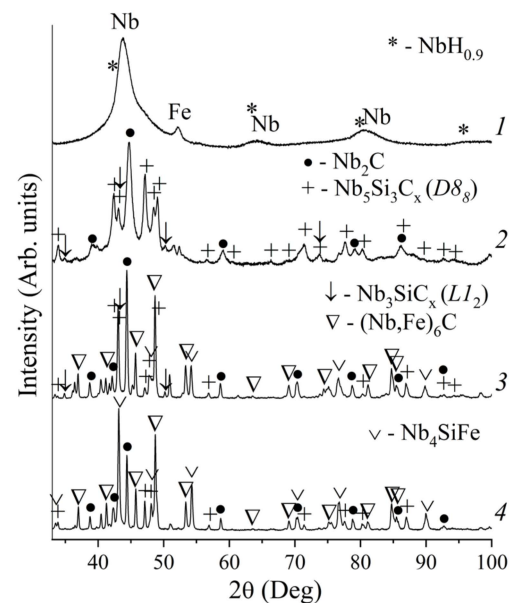
Figure 12. XRD patterns of sample *NbSi*: (*1*) MA powder; (*2*, *3*) MA powder annealed at (*2*) 900 °C, (*3*) 1000 °C, and (*4*) 1300 °C. MA duration is 4 h.

(**a**) (**b**)
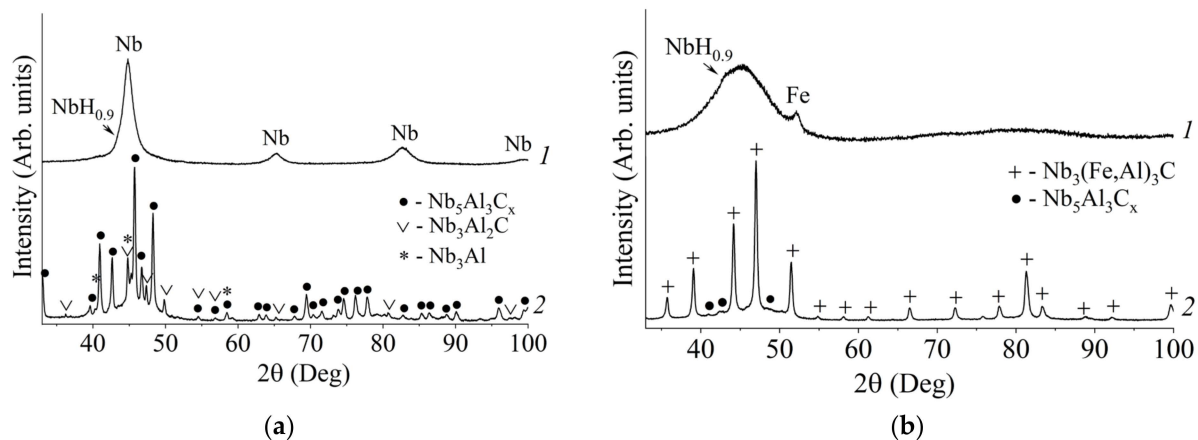
Figure 13. (**a**) XRD patterns of sample *NbAl*: (*1*) MA powder; (*2*) MA powder annealed at 900 °C. MA duration is 2 h. (**b**) XRD patterns of sample *NbAlFe*: (*1*) MA powder; (*2*) MA powder annealed at 900 °C. MA duration is 5 h.

Upon being added to the Nb-Al-C system, iron is dissolved in niobium with the formation of an X-ray amorphous phase (sample *NbAlFe*, Figure 13b). Annealing at 900 °C causes the formation of η-carbide $Nb_3(Fe,Al)_3C$, in addition to $Nb_5Al_3C_x$. η-carbide forms from an X-ray amorphous phase. Apparently, $(Nb,Fe)_6C$ phase is formed in a similar way. It should be noted that $Nb_3(Fe,Al)_3C$ carbide has been synthesized using wet ball milling for the first time.

All the obtained results indicate that wet milling in the steel equipment for even a comparatively short duration induces the decomposition of hydrocarbon, the formation of hydrides and carbohydrides, and the Fe contamination of the powders milled. Carbon accumulating in powders from milling media is involved in the formation of carbides and stabilization of metastable intermetallic compounds, whereas iron appearing due to milling equipment abrasion facilitates the formation of multicomponent phases with the structure of η-carbides.

4. Conclusions

1. The paper presents opportunities and advantages of wet ball milling for the mechanochemical synthesis of titanium-, niobium-, and tungsten-based carbohydrides and carbides, including those with added *d*-metals (Fe, Cu) or *p*-elements (Si, Al). The technique allows one to prepare multicomponent carbides, as well as metastable and high-temperature carbon-stabilized intermetallics as practically single phases, owing to the high-efficiency mixing of the elements, rapid nanostructuring of the powders milled, and homogeneous distribution of carbon accumulated by the powders from liquid hydrocarbon. The carbon concentration needed for the phase formation is easily governed by milling time.

2. The paper reports the results on the formation of the structural phase composition of the powders under mechanochemical synthesis, subsequent annealing, compaction, and application as coatings. The density, hardness, and wear resistance of compacts and coatings have been measured and analyzed.

3. It has been revealed that wet ball milling is accompanied by the following phase transformations: In the first stage, thermocatalytic decomposition of hydrocarbon in titanium- and niobium-based systems has been found to result in a supersaturated solid solution of carbon and hydrogen in the metal followed by the formation of hydride. Accumulation of carbon in powders under further milling facilitates the formation of metal carbohydride with a lattice close to that of carbide. In the tungsten-based system, only a supersaturated solid solution is formed because of the easy decomposability of hydride, and carbohydride is not formed or is easily decomposed.

4. The phase decomposition of the supersaturated solid solution and carbohydride under subsequent thermal treatment gives one- and/or multicomponent carbides (TiC, NbC, Nb_2C, $(Nb,Fe)_6C$, $(Nb,Al,Fe)_6C$, $(W,Fe)_6C$, $(W,Fe)_{12}C$). It has been shown that milling in steel equipment enables obtaining multicomponent η-carbides because of iron contamination.

5. In Ti–Si, Nb–Cu, Nb–Si, and Nb–Al systems, further thermal treatment has been shown to give metastable or high-temperature interstitial carbon-stabilized intermetallics with $D8_8$ and $L1_2$ structures ($Ti_5Si_3C_x$, $Nb_5Si_3C_x$, $Nb_5Al_3C_x$, Nb_3SiC_x, $Nb_3(Fe,Cu)C_x$). It should be noted that bulk carbon-stabilized $Nb_3(Fe,Cu)C_x$ and $Nb_5Al_3C_x$ intermetallics with $L1_2$ and $D8_8$ structures, respectively, have been obtained for the first time.

6. The wet-milled powders have been used to prepare compacts and coatings that exhibit high wear resistance. Coatings based on titanium, niobium, or bimetallic tungsten carbides are similar to industrial sintered WC-6Co alloy in their dry wear resistance.

Author Contributions: Conceptualization, S.L.; writing—original draft preparation, M.E. and S.L. All authors have read and agreed to the published version of the manuscript.

Institutional Review Board Statement: Not applicable.

Informed Consent Statement: Not applicable.

Data Availability Statement: Not applicable.

Conflicts of Interest: The authors declare no conflict of interest.

References

1. Shabalin, I.L. *Ultra-High Temperature Materials II. Refractory Carbides I (Ta, Hf, Nb and Zr Carbides). A Comprehensive Guide and Reference Book*; Springer: Singapore, 2019. [CrossRef]
2. Anasori, B.; Gogotsi, Y. *2D Metal Carbides and Nitrides (MXenes). Structure, Properties and Applications*; Springer Nature: Cham, Switzerland, 2019. [CrossRef]
3. Lomayeva, S.F.; Maratkanova, A.N. Structure, phase composition and magnetic properties of Fe-Si-C system due to mechanical activation of Fe-Si alloy in organic liquids. *Intermetallics* **2009**, *17*, 714–721. [CrossRef]
4. Yazovskikh, K.A.; Lomayeva, S.F. Mechanosynthesis of Fe-NbC nanocomposite. *J. Alloys Compd.* **2014**, *586* (Suppl. 1), S65–S67. [CrossRef]
5. Shcherbakov, V.A.; Gryadunov, A.N.; Semenchuk, I.E.; Kovalev, D.Y.; Sychev, A.E.; Alymov, M.I. Synthesis of Ta_4HfC_5 ceramics with a submicron structure by electro-thermal explosion under pressure. *Dokl. Chem.* **2021**, *501*, 259–263. [CrossRef]
6. Qian, C.; Liu, Y.; Cheng, H.; Li, K.; Liu, B. Effect of the carbon content on the morphology evolution of the η phase in cemented carbides with the CoNiFeCr high entropy alloy binder. *Int. J. Refract. Met. Hard Mater.* **2022**, *102*, 105731. [CrossRef]
7. Boltachev, G.S.; Nagayev, K.A.; Paranin, S.N.; Spirin, A.V.; Volkov, N.B. Theory of the magnetic pulsed compaction of nanosized powders. In *Nanomaterials: Properties, Preparation and Processes*; Nova Science Publishers, Inc.: New York, NY, USA, 2011; pp. 1–58.
8. Kharanzhevskiy, E.; Ipatov, A.; Nikolaeva, I.; Zakirova, R. Short-pulse laser sintering of multilayer hard metal coatings: Structure and wear behavior. *Lasers Manuf. Mater. Proc.* **2015**, *2*, 91–102. [CrossRef]
9. Shelekhov, E.V.; Sviridova, T.A. Programs for X-ray analysis of polycrystals. *Met. Sci. Heat Treat.* **2000**, *42*, 309–313. [CrossRef]
10. Khidirov, I. *Neutron Diffraction Study of Hydrogen Thermoemission Phenomenon from Powder Crystals, Neutron Diffraction*; InTech: Rijeka, Croatia, 2012; ISBN 978-953-51-0307-3. Available online: http://www.intechopen.com/books/neutron-diffraction/neutron-diffraction-study-of-hydrogen-thermoemissionphenomenon-from-powder-crystals (accessed on 15 December 2019).
11. Dolukhanyan, S.K.; Aghajanyan, N.N.; Hakobyan, H.G.; Shekhtman, V.S.; Ter-Galstyan, O.P. The structural peculiarities of the transition metals carbohydrides produced by combustion synthesis. *J. Alloys Compd.* **1999**, *293–295*, 452–457. [CrossRef]
12. Renaudin, G.; Yvon, K.; Dolukhanyan, S.K.; Aghajanyan, N.N.; Shekhtman, V.S. Crystal structures and thermal properties of titanium carbo-deuterides as prepared by combustion synthesis. *J. Alloys Compd.* **2003**, *356–357*, 120–127. [CrossRef]
13. Dorofeev, G.A.; Lad'yanov, V.I.; Lubnin, A.N.; Mukhgalin, V.V.; Kanunnikova, O.M.; Mikhailova, S.S.; Aksenova, V.V. Mechanochemical interaction of titanium powder with organic liquids. *Int. J. Hydrogen Energy* **2014**, *39*, 9690–9699. [CrossRef]
14. $Ti_2CH_{0.6}$ Crystal Structure. Available online: https://materials.springer.com/isp/crystallographic/docs/sd_1705239 (accessed on 15 October 2019).
15. Eremina, M.A.; Lomaeva, S.F.; Burnyshev, I.N.; Kalyuzhnyi, D.G. Mechanosynthesis of precursors for TiC-Cu cermets. *Russ. Phys. J.* **2018**, *60*, 2155–2163. [CrossRef]
16. Eremina, M.A.; Lomaeva, S.F.; Paranin, S.N.; Tarasov, V.V. Influence of mechanoactivation conditions and surfactant addition on phase composition and properties of titanium carbohydride—Copper composites. *Phys. Met. Metallogr.* **2020**, *121*, 180–187. [CrossRef]
17. Rocha, S.S.; Adabo, G.L.; Henriques, G.E.P.; Nobilo, M.A.A. Vickers hardness of cast commercially pure titanium and Ti-6Al-4V alloy submitted to heat treatments. *Braz. Dent. J.* **2006**, *17*, 126–129. [CrossRef]
18. Eryomina, M.A.; Lomayeva, S.F.; Kharanzhevskiy, E.V.; Burnyshev, I.N. Peculiarities of phase formation in the mechanosynthesized titanium carbohydride powders under short pulse selective laser alloying. *Eur. Phys. J. Special Top.* **2019**, *228*, 2429. [CrossRef]
19. Eryomina, M.A.; Lomayeva, S.F.; Kharanzhevskiy, E.V. Structure and wear resistance of coatings produced by the short-pulse laser alloying of titanium carbohydride-based mechanocomposites. *Powder Metall. Funct. Coat.* **2021**, *4*, 46–56. [CrossRef]
20. Eryomina, M.A.; Lomayeva, S.F. Mechanosynthesis of TiC(NbC)–Cu composites using liquid hydrocarbons. *Mater. Today Proc.* **2019**, *12*, 151–154. [CrossRef]
21. Eryomina, M.A.; Lomayeva, S.F.; Demakov, S.L.; Yurovskikh, A.S. SPS of "Titanium carbide/carbohydride–copper" Composites. In Proceedings of the XIX International Scientific-Technical Conference "The Ural School-Seminar of Metal Scientists-Young Researchers", Yekaterinburg, Russia, 19–23 November 2018; pp. 246–252. [CrossRef]
22. Liu, H.; Zhang, J.; Sun, P.; Zhou, C.; Liu, Y.; Fang, Z.Z. Effect of oxygen addition on phase composition and activation properties of TiFe alloy. *Int. J. Hydrogen Energy* **2023**, *48*, 8563–8572. [CrossRef]
23. Holleck, H. *Binäre und Ternäre Carbide und Nitride der Übergangsmetalle und ihre Phasenbeziehungen*; Kernforschungszentrum Karlsruhe GmbH: Karlsruhe, Germany, 1981.
24. Eryomina, M.A.; Lomayeva, S.F.; Demakov, S.L. Synthesis of titanium carbosilicides in Ti-Si and Ti-Si-Cu systems under mechanical alloying of elemental powders in liquid hydrocarbon. *J. Sol. St. Chem.* **2020**, *290*, 121575. [CrossRef]
25. Eryomina, M.A.; Lomayeva, S.F.; Lyalina, N.V.; Syugaev, A.V.; Paranin, S.N.; Tarasov, V.V. Structure and properties of mechanosynthesized W-Fe-C carbides. *Mater. Today Proc.* **2020**, *25*, 356–359. [CrossRef]
26. Eryomina, M.A.; Lomayeva, S.F.; Kharanzhevsky, E.V.; Tarasov, V.V.; Dementyev, V.B. Phase composition and wear resistance of compacts and coatings based on carbides fabricated in W-Fe-C system by wet mechanical alloying. *Proc. Struct. Integr.* **2021**, *32*, 284. [CrossRef]

27. Eryomina, M.A.; Lomayeva, S.F.; Kharanzhevsky, E.V.; Bel'tyukov, A.N. Wear-resistant coatings produced by high-speed selective laser sintering of wet-milled W-Fe powders: Phase composition, microstructure, and properties. *Int. J. Refract. Met. Hard Mater.* **2022**, *108*, 105915. [CrossRef]

28. Dash, T.; Nayak, B.B. Preparation of WC-W_2C composites by arc plasma melting and their characterizations. *Ceram. Int.* **2013**, *39*, 3279–3292. [CrossRef]

29. Dvornik, M.; Mikhailenko, E.; Nikolenko, S.; Vlasova, N.; Skiruta, A. Production of ultrafine-grained spherical β-WC-W_2C-Co microparticles by electro discharge erosion of WC-15Co alloy in glycerol and their solutions. *Mater. Res. Express* **2020**, *7*, 096504. [CrossRef]

30. Eryomina, M.A.; Lomayeva, S.F.; Kharanzhevsky, E.V.; Tarasov, V.V.; Burnyshev, I.N. Wet ball milling and subsequent high-speed selective laser sintering of Nb-Cu powders for applying wear-resistant coatings. *Int. J. Refract. Met. Hard Mater.* **2022**, *105*, 105837. [CrossRef]

31. Timokhina, I.B.; Enomoto, M.; Miller, M.K.; Pereloma, E.V. Microstructure-property relationship in the thermomechanically processed C-Mn-Si-Nb-Al-(Mo) transformation-induced plasticity steels before and after prestraining and bake hardening treatment. *Met. Mater. Trans. A* **2012**, *43*, 2473–2483. [CrossRef]

32. Materials Explorer. Nb_3Fe: mp-999440. Available online: https://materialsproject.org/materials/mp-999440 (accessed on 3 February 2023).

33. Neu, V.; Crespo, P.; Schäfer, R.; Eckert, J.; Schultz, L. High remanence Nd-Fe-B-X (X = Cu, Si, Nb_3Cu, Zr) powders by mechanical alloying. *J. Magn. Magn. Mater.* **1996**, *157–158*, 61–62. [CrossRef]

34. Dai, Y.; Kong, Y.; Li, J.H.; Liu, B.X. Structural stability of high-pressure phase in the immiscible Cu-Nb system studied by lattice dynamics calculation. *J. Alloys Compd.* **2009**, *468*, 299–302. [CrossRef]

35. Opahle, I.; Singh, H.K.; Zemen, J.; Gutfleisch, O.; Zhang, H. Effect of N, C, and B interstitials on the structural and magnetic properties of alloys with Cu_3Au structure. *Phys. Rev. Res.* **2020**, *2*, 023134. [CrossRef]

36. Pan, Y. Prediction of new structure, phase transition, mechanical, and thermodynamic properties of Nb_3Si. *Adv. Eng. Mater.* **2017**, *19*, 1700099. [CrossRef]

37. Fahmy, Y.; Benfield, C.T.; Koch, C.C. The effects of interstitial elements on the phase stability and mechanical behavior of selected intermetallics. *Mater. Sci. Eng. A* **1993**, *170*, 19–27. [CrossRef]

38. Scabarozi, T.H.; Roche, J.; Rosenfeld, A.; Lim, S.H.; Salamanca-Riba, L.; Yong, G.; Takeuchi, I.; Barsoum, M.W.; Hettinger, J.D.; Lofland, S.E. Synthesis and characterization of Nb_2AlC thin films. *Thin Solid Films* **2009**, *517*, 2920–2923. [CrossRef]

39. Kohmoto, H.; Shyue, J.; Aindow, M.; Fraser, H.L. Observation of a metastable B2 phase in rapidly solidified ribbons of Nb-Al alloys. *Scr. Metall. Mater.* **1993**, *29*, 1271–1274. [CrossRef]

40. Wang, X.; Yang, J.; Zhang, K.; Hu, R.; Song, L.; Fu, H. Atomic-scale observations of B2→ω-related phases transition in high-Nb containing TiAl alloy. *Mater. Charact.* **2017**, *130*, 135–138. [CrossRef]